Growth of a needle crystal from an undercooled alloy melt

M. Conti
Dipartimento di Matematica e Fisica, Università di Camerino, 62032 Camerino, Italy
(Received 3 December 1996; revised manuscript received 14 April 1997)

The growth of a free dendrite from a supercooled alloy melt is studied with the phase-field model in the isothermal approximation; the surface tension is assumed to be asymmetric with fourfold anisotropy. For fixed supercooling and when the anisotropy parameter γ is not too high, the computed tip radius ρ and velocity $v_{\rm tip}$ obey the scaling law $\rho^2 v_{\rm tip} \propto \gamma^{-7/4}$, predicted by the microscopic solvability theory. The solute diffusion across the solid-liquid interface reflects the nonequilibrium conditions of the growth process: the concentration jump deviates from the static value and decreases with increasing interface velocity. We also explore the effect of different diffusivities in the solid and liquid phases. Previous studies based on the equilibrium formulation of the free boundary equations predict a monotonic increase of $\rho^2 v_{\rm tip}$ with the solute diffusivity of the solid phase; due to nonequilibrium effects this result is not recovered in the present investigation. [S1063-651X(97)01309-3]

PACS number(s): 64.70.Dv, 68.10.Gw, 81.30.Bx, 82.65.Dp

I. INTRODUCTION

The steady growth of a needle-shaped crystal from its supercooled melt has been addressed in several studies; extensive reviews are given in [1–3]. The dynamic evolution of the process is the result of a competition between the nonequilibrium conditions imposed at infinity and the necessity to reject at least one conserved quantity away from the advancing front. For pure substances the growth is controlled by the diffusion of the latent heat released at the solid-liquid interface ; for binary alloys the relaxation of the thermal field is much faster than the rearrangement of chemical species, so that the limiting mechanism is solute diffusion and the growth process is generally treated as isothermal. Langer [4] pointed out that, considering the chemical potential rather than the solute concentration as the diffusive field, the chemical and the thermal versions of the free boundary diffusional model can be formally mapped onto the same set of governing equations. To be consistent with the discussion and the results presented in the subsequent sections, in the following we will adopt the language of the chemical model.

The selection mechanism of the dendrite operating point has intrigued the scientific community for a long time. A satisfactory theory should relate both the dendrite tip radius ρ and the velocity $v_{\rm tip}$ to the conditions imposed at infinity, namely, the dimensionless supercooling $\Delta = (c_l^* - c_\infty)/(c_l^* - c_s^*)$, where c_∞ represents the initial solute concentration of the melt and c_l^* and c_s^* are the equilibrium solute concentrations on the liquid side and the solid side of the interface, respectively. The parabolic solution, discovered by Ivantsov [5], neglecting capillary effects, can only determine the Péclet number $P = \rho v_{\rm tip}/2D$ as a function of Δ (D is the solute diffusivity), i.e., neither $v_{\rm tip}$ nor ρ is uniquely fixed, but only their product. The degeneracy of this solution is due to the lack of the necessary length scale for the pattern description. This deficiency can be removed taking into account the effects of a finite surface tension σ, which introduces in the model the capillary length d_0; for dilute solutions the latter can be defined as $d_0 = \sigma T_A / m L_A \Delta c$, T_A and L_A being the melting temperature and the latent heat of the solvent, respectively; $m = dT/dc$ is the liquidus slope on the T,c representation of the phase diagram and $\Delta c = (c_l^* - c_s^*)$. From this perspective, a solvability approach [6–10] indicates that for a stable and steady tip propagation surface energy is not sufficient and anisotropy of the surface energy is required; moreover, it allows one to identify the dendrite operating point, fixing the value of the so-called stability constant $\sigma^* = d_0 D/\rho^2 v_{\rm tip}$. It was shown that, at low values of the anisotropy parameter γ (defined below), the solvability condition imposes $\sigma^* \sim \gamma^{7/4}$.

All these studies were conducted starting from the free boundary equations, generally written in the thermal formulation; due to mathematical tractability the boundary conditions on the solidification front reflected the assumption of local thermodynamic equilibrium. However, as pointed out by Ben Amar [10], this approximation is no longer valid in rapid solidification processes and yields a strong overestimate of the growth velocity at large values of Δ.

To overcome the above difficulty, the growth of a free dendrite can be addressed through the phase-field model (PFM). A phase field $\phi(x,t)$ characterizes the phase of the system at each point. A free-energy (or entropy) functional is then constructed that depends on ϕ as well as on the temperature and concentration fields; a $(\nabla\phi)^2$ term accounts for the energy cost associated with the solid-liquid interface. The extremization of the functional with respect to these variables results in the dynamic equations for the evolution of the process. This approach was pioneered by Caginalp in a series of studies [11–15] and was initially applied to the solidification of pure substances. In recent years the PFM has been extended to describe the solidification of binary alloys [16–20].

Wheeler, Boettinger, and McFadden [16] addressed alloy solidification in the isothermal approximation and conducted an asymptotic analysis of the governing equations for a vanishlingly small interface thickness. The results they found predicted an increase of the interface concentration jump with increasing the interface velocity; on the contrary, rapid solidification experiments show that solute segregation on

the moving front is suppressed at large growth rates (a phenomenon that is termed ''solute trapping''). In a successive study Wheeler, Boettinger, and McFadden [17] recovered a consistent description of the solute segregation through an *ad hoc* modification of the model, inserting into the free-energy functional a $(\nabla c)^2$ correction acting to oppose the sharp transition of the solute profile across the interface.

Caginalp and Xie [18] and Caginalp and Jones [19] rephrased the simpler and more natural version of the model, without the $(\nabla c)^2$ term, and identified through an asymptotic analysis the sharp interface limit of the phase-field equations; in this limit both the Gibbs-Thompson effect and the interface kinetic undercooling at large velocities are properly described. Subsequently, Conti [21,22] showed that for small but finite interface thickness the model is also capable of predicting solute trapping.

In the present paper the phase-field model, in the formulation presented by Caginalp and Jones [19], is utilized to simulate the growth of a needle crystal in two dimensions. It is the aim of this study to determine how and to what extent nonequilibrium effects contribute to alter the picture of the process given in previous studies that, due to mathematical difficulties, were based on the equilibrium formulation of the free boundary model.

II. PHASE-FIELD MODEL

A. Governing equations

The model describes the solidification of an ideal solution of components A (solvent) and B (solute) in terms of two fields: the scalar phase field ϕ and the local solute concentration c. Assuming heat diffusion much faster than solute diffusion, the isothermal approximation is allowed. The field ϕ is an order parameter assuming the values $\phi=0$ in the solid and $\phi=1$ in the liquid at equilibrium; intermediate values correspond to the interface between the two phases. The model is developed along the lines suggested by Caginalp and Jones [19]; the simultaneous variations of a free-energy functional with respect to the two fields give the dynamic equations

$$\tau\frac{\partial\phi}{\partial t}=BT\nabla^2\phi-\alpha T\phi(1-\phi)\left(\frac{1}{2}-\phi\right)-q(\phi)\left[cL_B\left(1-\frac{T}{T_B}\right)+(1-c)L_A\left(1-\frac{T}{T_A}\right)\right], \tag{1}$$

$$\frac{\partial c}{\partial t}=\nabla\cdot\left\{D\nabla c+Dc(1-c)\frac{v_m}{RT}\times\left[L_B\left(1-\frac{T}{T_B}\right)-L_A\left(1-\frac{T}{T_A}\right)\right]\nabla\phi\right\}. \tag{2}$$

The standard version of the model corresponds to the choice $q(\phi)=1$ in Eq. (1). However, for numerical convenience, we decided to force the order parameter to the values $\phi=0$ and 1 in the bulk phases even in nonequilibrium conditions; this can be obtained with $q(\phi)=30\phi^2(\phi-1)^2$ [20]. Though this choice cannot be correctly based on a microscopical interpretation of the process, we observed that the numerical results were not significantly affected. In Eq. (2) R is the gas constant and v_m the molar volume; L_A, T_A, L_B, T_B represent the latent heat and the melting temperature of pure A and B, respectively. The model parameters α, B, τ are related to the material properties through the relations [19]

$$\alpha=\frac{12\sigma}{\epsilon T}, \tag{3}$$

$$B=\frac{6\sigma\epsilon}{T}, \tag{4}$$

$$\tau=\frac{6\epsilon L_A}{\mu_A T_A}, \tag{5}$$

where ϵ is the thickness of the solid-liquid interface and μ_A is the kinetic undercooling coefficient that relates, for a pure substance, the interface undercooling to the interface velocity through $v=\mu_A(T_A-T)$.

To allow for different diffusivities in the solid and liquid phases, in the following D will be taken as

$$D=D_s+\phi(D_l-D_s), \tag{6}$$

D_l and D_s being the diffusivities in the liquid and in the solid, respectively. Anisotropy can be inserted in the model following the ideas of [23]; scaling lengths to some reference scale ξ and time to ξ^2/D_l, the model equations become

$$\frac{\partial\phi}{\partial t}=m\times\left\{\nabla\cdot[\eta^2(\theta)\nabla\phi]+\frac{\partial}{\partial y}\left(\eta(\theta)\eta'(\theta)\frac{\partial\phi}{\partial x}\right)-\frac{\partial}{\partial x}\left(\eta(\theta)\eta'(\theta)\frac{\partial\phi}{\partial y}\right)-\frac{2}{\tilde{\epsilon}^2}\phi(1-\phi)\left(\frac{1}{2}-\phi\right)+\frac{1}{6\tilde{\epsilon}}q(\phi)[c\tilde{G}_B+(1-c)\tilde{G}_A]\right\}, \tag{7}$$

$$\frac{\partial c}{\partial t}=\nabla\cdot[\lambda(\phi)\nabla c+\lambda(\phi)c(1-c)(\tilde{H}_A-\tilde{H}_B)\nabla\phi], \tag{8}$$

where

$$\tilde{G}_{A,B}=\frac{\xi}{\sigma}\frac{L_{A,B}}{T_{A,B}}(T-T_{A,B}), \tag{9}$$

$$\tilde{H}_{A,B}=\frac{v_m}{RT}\frac{L_{A,B}}{T_{A,B}}(T-T_{A,B}), \tag{10}$$

$$m=\frac{\mu_A\sigma T_A}{D_l L_A}, \tag{11}$$

$$\tilde{\epsilon}=\frac{\epsilon}{\xi} \tag{12}$$

and $\lambda(\phi)$ is defined as

TABLE I. Material parameters for the Ni-Cu alloy.

Parameter	Nickel	Copper
T_m (K)	1728	1358
L (J/cm^3)	2350	1728
v_m (cm^3/mole)[a]	7.0	7.8
σ (J/cm^2)	3.7×10^{-5}	2.8×10^{-5}
β (cm/K s)[b]	160	198
D_l (cm^2/s)	10^{-5}	10^{-5}

[a]An average value of 7.4 has been taken.
[b]From the estimation of Willnecker, Herlach, and Feuerbacher (Ref. [31]).

$$\lambda(\phi)=\frac{D_s}{D_l}+\phi\left(1-\frac{D_s}{D_l}\right). \tag{13}$$

In Eq. (7) θ is the angle between the normal to the interface and a fixed direction (the x axis in our calculations); choosing the function $\eta(\theta)=(1+\gamma\cos4\theta)$, a fourfold anisotropy of the surface tension is enforced, with γ specifying the intensity of the effect.

B. Computational approximations

To conduct the numerical simulations we referred to the thermophysical properties of an ideal solution of nickel (solvent) and copper (solute), summarized in Table I. However, due to limitations of computational resources, we were forced to use some approximations elucidated below.

In two dimensions the numerical cost of the solution is dramatically dependent on the interface thickness, increasing as ϵ^{-4}. In this study, along the lines suggested by Caginalp and Socolovsky [15], a value is selected for the interface thickness that is small compared to the lowest geometric scale that characterizes the process, namely, the radius of curvature of the dendrite tip and, nevertheless, more than ten times greater than realistic values.

The diffusivities of the phase and the concentration fields are quite different and Eqs. (7) and (8) should be discretized with different resolution in the time domain, with the finer grid fixing the numerical cost. To overcome this difficulty and to allow a coarser time grid, we decided to reduce the diffusivity of the phase field in Eq. (7), choosing a value for $D_l$about 10^2 times the actual value (notice that mass diffusion is still modeled as a process much slower than heat diffusion). Moreover, to allow the growth of the needle crystal in a space domain of reasonable size, the surface tension of both the materials was reduced by a factor 2.5. As we fixed the temperature of the melt at $T=1574$ K and the length scale at $\xi=2.1\times10^{-4}$ cm, the model parameters become $\tilde{\epsilon}=2.8\times10^{-2}$, $m=0.6$, $\tilde{G}_A=-3273$, $\tilde{G}_B=4263$, $\tilde{H}_A=-0.1184$, and $\tilde{H}_B=0.1554$.

III. NUMERICAL METHOD

Equations (7) and (8) have been solved on a computational domain $0\leqslant x\leqslant x_m$, $0\leqslant y\leqslant y_m$; choosing $x_m=y_m=4$ was enough to prevent finite-size effects. Neumann conditions were imposed at the domain's boundaries. Initially, in the uniform undercooled melt ($c=c_\infty$, $\phi=1$), a semicircular solid germ ($c=c_\infty$, $\phi=0$), is nucleated, with the center at $x=0$, $y=y_m/2$ and radius $R_0=0.1$. The germ's surface is perturbed by a random corrugation; at the early stage of the growth the high-frequency components of the perturbation coalesce and the pattern selected by the system is a single dendrite that propagates into the channel along the x axis.

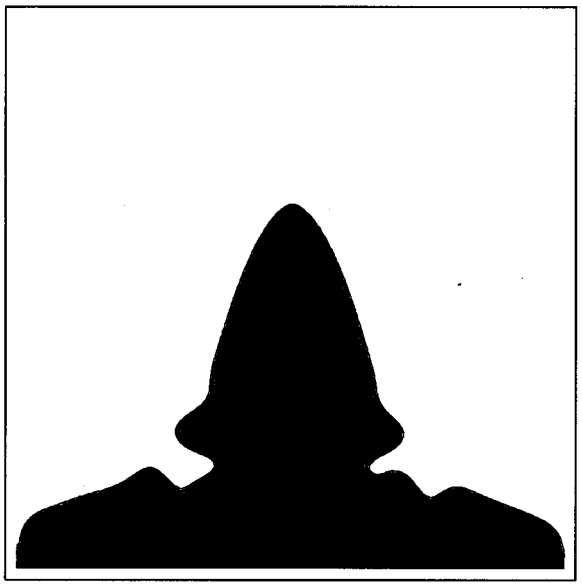

FIG. 1. Needle crystal at $t=0.07$; the anisotropy parameter is $\gamma=0.035$.

An explicit Euler integration scheme was employed to advance the solution forward in time; second-order central differences were used to discretize the Laplace operator. To ensure an accurate resolution of both the phase and the concentration profiles the grid spacing was selected as $\Delta x=\Delta y=6.25\times10^{-3}$; with these values no preferred directions emerge in the computational grid, due to the truncation errors. A time step $\Delta t=0.125\times10^{-4}$ was required for numerical stability. To verify the consistency of the numerical scheme, at each time step the solute conservation was checked and in all the simulations was verified within 0.001%.

IV. NUMERICAL RESULTS

At the melt temperature $T=1574$ K the equilibrium solute concentrations in the bulk phases are $c_s^*=0.399\,09$ and $c_l^*=0.466\,24$. As we fixed $c_\infty=0.408\,49$, the initial supercooling is $\Delta=0.86$.

As a default we set $D_s=D_l$; successively we will present the effects of a nonsymmetric diffusion in the two phases. Except for temperature, dimensionless units will be used throughout this section.

With anisotropic surface tension, a distinct needle crystal grows along the x axis; a typical example of this behavior is shown in Fig. 1. For $\gamma>9\times10^{-3}$, after a transient that becomes shorter as γ increases, the dendrite tip propagates at constant velocity. Below this value we did not succeed in identifying a steady growth regime, probably due to the short period of computation and the small system size.

First we will examine the morphology of the crystal with

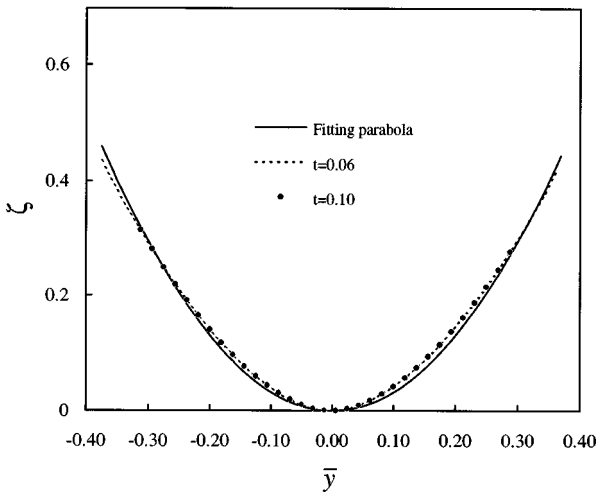

FIG. 2. Two snapshots of the crystal's interface in a frame of reference centered at the dendrite tip. The solid line represents the best fitting parabola $\zeta(\overline{y})=a\overline{y}^2$; $\gamma=0.02$.

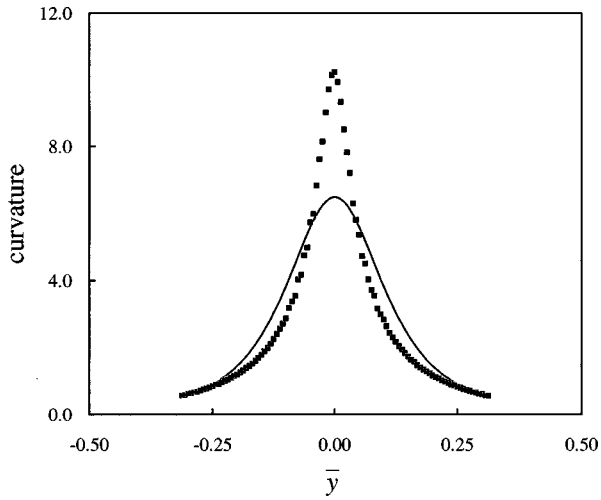

FIG. 3. Curvature of the solid-liquid interface (squares), compared to that of the best-fitting parabola (solid curve); $\gamma=0.02$ and $t=0.1$.

respect to the predictions of existing models. In a frame of reference moving with the tip, the interface [defined as the locus $\phi(x,y,t)=0.5$] is described by an even function $\zeta(\overline{y})$ of the shifted coordinate $\overline{y}=y-y_{\rm tip}$. Figure 2 shows $\zeta(\overline{y})$ at two different times (here $\gamma=0.02$). We observe that in the region $|\overline{y}|\leqslant 0.3$ and for $t\geqslant 0.06$ the dendrite tip preserves its shape.

The free boundary diffusional model, neglecting surface tension and nonequilibrium effects, admits a solution of the form [5]

$$\zeta(\overline{y})=a\overline{y}^2, \tag{14}$$

where a is related to the tip velocity and the initial supercooling through

$$\Delta=\sqrt{\frac{\pi v_{\rm tip}}{4a}}\exp\left(\frac{v_{\rm tip}}{4a}\right)\operatorname{erfc}\left(\sqrt{\frac{v_{\rm tip}}{4a}}\right). \tag{15}$$

Trying to adapt the above solution to the interface position at $t=0.1$, a least-squares fit indicated a best value of $a=3.26$. The fitting parabola is superimposed on the curves of Fig. 2. Using the numerically computed value of the tip velocity $v_{\rm tip}=29.8$, Eq. (15) yields $\Delta=0.856$, which is quite close to the actual value $\Delta=0.86$.

Figure 3 shows, as a function of $\overline{y}$, the curvature of the fitting parabola compared to that of the actual interface, the latter being determined numerically through the relation

$$\mathcal{K}=\frac{\zeta''(\overline{y})}{(1+\zeta'^2)^{3/2}}. \tag{16}$$

We observe in the tip region a marked increase of the actual curvature, beyond the values predicted by Eq. (14); the inability to describe the interface through a parabolic curve near the tip has to be ascribed to the perturbations introduced by capillary and nonequilibrium effects.

Let us now examine the solute distribution across the interface. It is well known that in rapid solidification processes the partition coefficient $k=c_s/c_l$ ($c_s$and c_l being the solute concentration on the solid and the liquid side of the interface, respectively) deviates from the equilibrium value k_e increasing towards unity at large interface velocities. This phenomenon, termed *solute trapping*, was explained by Aziz [24], Aziz and Kaplan [25], and Aziz and Boettinger [26] within the continuous growth model, as a result of a diffusive redistribution of solute and solvent across the interface. They found a dependence

$$k(v)=\frac{k_e+v/v_d}{1+v/v_d}, \tag{17}$$

where v_d is a characteristic kinetic velocity, which is often taken as D/ℓ, D being the interface diffusivity and ℓ the interface width. For a shape-preserving curve $\zeta(\overline{y})$, the normal interface velocity, as a function of $\overline{y}$, is given by

$$v=\frac{v_{\rm tip}}{\sqrt{1+\zeta'^2}}. \tag{18}$$

Using Eqs. (17) and (18), it is possible to evaluate $k(v)$ along the two branches of the interface. Preliminarily we have to fix the interface width ℓ.

Figure 4 shows, along the crystal axis, the solute concentration profile normalized as $\overline{c(x)}=[c(x)-c_{\rm min}]/(c_{\rm max}-c_{\rm min})$, where $c_{\rm min}$ and $c_{\rm max}$are the minimum and maximum values of $c(x)$ along the x axis. We observe that $\overline{c(x)}$ jumps from 10% to 90% of its maximum value within a length of order $\ell=0.044$; then we fix this value as the interface width. Choosing the interface diffusivity as $D=D_s=D_l$ results in $v_d=23$. Figure 5 shows the partition coefficient k evaluated through Eqs. (17) and (18) as a function of $\overline{y}$; on the same graph we represented the ratio c_s/c_l as resulting from the numerical simulation. The agreement between the two curves is quite good. It is worth observing that Eq. (17) conveys no information about the interface curvature (the Gibbs-Thomson effect predicts an *increase* of $k$departing from the crystal tip [27]); then we see that the numerical results reflect the trapping of solute at the moving front. We now discuss the response of the growth dynamics to varia-

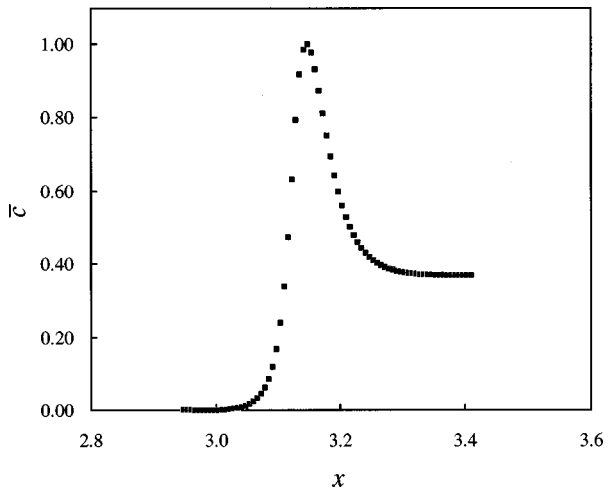

FIG. 4. Normalized concentration profile along the crystal's axis; $\gamma=0.02$ and $t=0.1$.

tions of the anisotropy strength γ. Starting from the free boundary formulation of the problem, Pelcè and Pomeau [28] established a nonlocal equation for the deviation of the interface profile from the Ivantsov's solution. As shown by Barbieri and Langer [8] and Ben Amar [10], the solvability condition that has to be satisfied requires that the product $\rho^2 v_{\rm tip}$ scales as $\gamma^{-7/4}$ for low values of γ. This result was confirmed for the solidification of a pure substance by the phase-field simulations of Wheeler, Murray, and Schaefer [29] and Marinozzi, Conti, and Marini Bettolo Marconi [30]. Figure 6 shows in a log-log plot $\rho^2 v_{\rm tip}$ versus γ. For $\gamma \leqslant 9\times10^{-3}$ the tip radius and velocity were computed at the end of the simulation, when a true steady regime had not yet been reached; the tip radius was determined evaluating the expression $\rho=\phi_x/\phi_{yy}$ on the dendrite axis, at the solid-liquid interface. The numerical data fit well the $\gamma^{-7/4}$ power law (solid line) for $\gamma \leqslant 0.02$. This result is somewhat surprising: as the concentration field is strongly influenced by solute trapping, one could expect a substantial deviation of the growth dynamics from the predictions of a model that discards nonequilibrium effects.

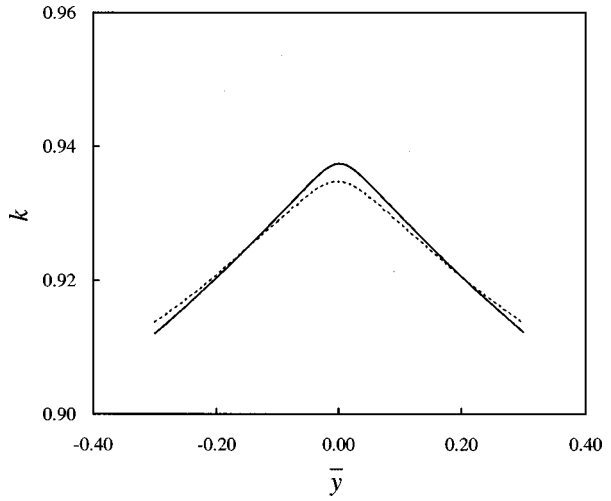

FIG. 5. Partition coefficient $k=c_s/c_l$ along the solid-liquid interface. Solid line, as derived through Eq. (17); dashed line, results of the numerical simulation. The anisotropy parameter is $\gamma=0.02$ and $t=0.1$.

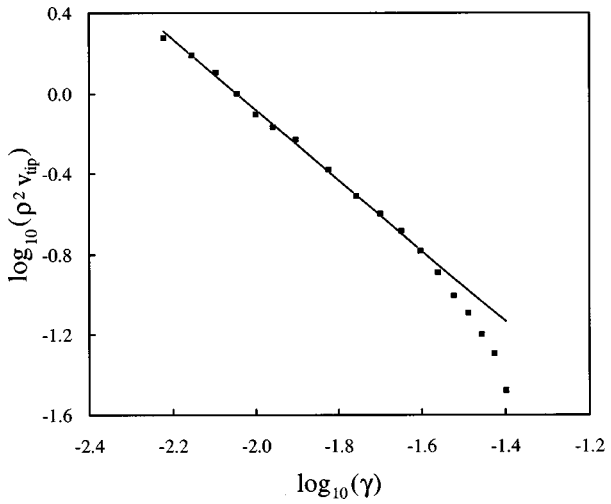

FIG. 6. A log-log plot of the product $\rho^2 v_{\rm tip}$ versus the anisotropy parameter γ. The super-imposed straight line corresponds to the power law $\rho^2 v_{\rm tip} \propto \gamma^{-7/4}$.

All the previous results were obtained assuming symmetric diffusion in the solid and liquid phases. This description could be adequate for thermal dendrites; however, when the diffusion field is the solute concentration, a more realistic approach should account for the lower mass diffusivity in the solid phase. Barbieri and Langer [8] utilized the free boundary equations, assuming local thermodynamic equilibrium, to show that the product $\rho^2 v_{\rm tip}$ depends on the ratio D_s/D_l as

$$\rho^2 v_{\rm tip}=\frac{1+D_s/D_l}{2}(\rho^2 v_{\rm tip})|_{D_s/D_l=1}. \tag{19}$$

The extension of this result to the chemical problem is not straightforward. For thermal dendrites, due to the Gibbs-Thomson effect, the growing solid is not isothermal and heat is driven towards the cold tip region. When diffusion in the solid phase is suppressed, the tip can propagate at larger velocity and [see Eq. (15)] the tip radius diminishes; as the product $\rho v_{\rm tip}$ depends only on Δ, $\rho^2 v_{\rm tip}$ diminishes as well. Taking into account the interface kinetics undercooling alters this picture quantitatively, but not qualitatively.

For chemical dendrites the situation is quite different. Curvature lowers the solute concentration near the tip, in the solid region; on the contrary, solute trapping, whose effect is maximal near the tip, is there a continuous source of solute. Notice that, along the two branches of the interface, the two effects decay in a different way. Figure 7 shows $c_s(\overline{y})$ for $D_s=0$ (triangles) and $D_s=D_l$ (squares); the accumulation of solute near the tip is clearly recognizable when diffusion in the solid is suppressed. Due to competition of these effects, it is not simple to predict the dependence of the growth dynamics on the ratio D_s/D_l. As shown in Fig. 8, contrary to the predictions of Eq. (19), $\rho^2 v_{\rm tip}$ decreases with increasing D_s/D_l.

V. CONCLUSIONS

The growth of a needle crystal into its undercooled melt is generally addressed through the free boundary diffusional model; the mechanism that underlies the selection of the tip

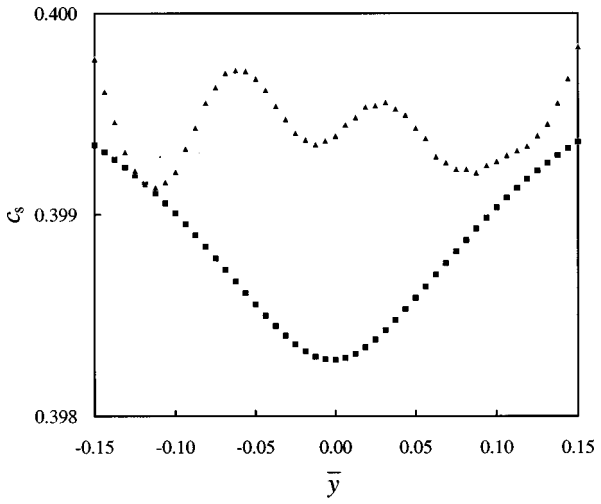

FIG. 7. Solute concentration on the solid side of the interface versus $\bar{y}$. Triangles, $D_s=0$; squares, $D_s=D_l$. The anisotropy parameter is $\gamma=0.02$ and $t=0.1$.

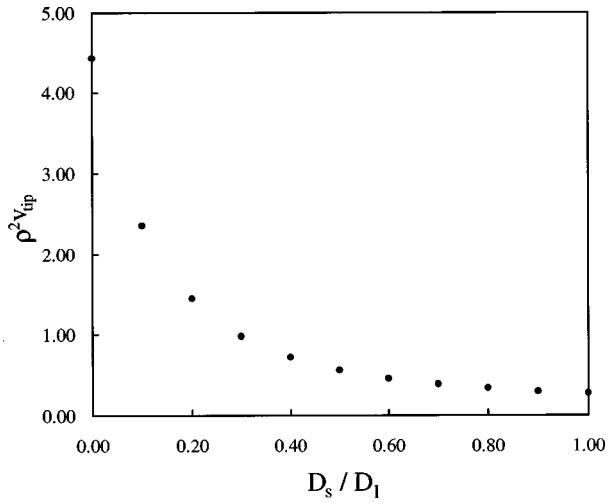

FIG. 8. Product $\rho^2 v_{\mathrm{tip}}$ versus the ratio D_s/D_l. The anisotropy parameter is $\gamma=0.02$.

radius and velocity has been identified under the approximation of local equilibrium at the solid-liquid interface. In this limit the same set of equations can formally describe the growth process when the diffusion field is either the melt temperature or the concentration of impurities. This similarity is no longer retained when in rapid solidification processes the interfacial equilibrium is broken, as solute trapping is a phenomenon that has no counterpart in the thermal problem. Through the phase-field model we were able to stress the nonequilibrium characteristics of the process. The system considered was a single dendrite growing into a supersaturated binary solution. The solute segregation across the moving front is essentially determined by the interface kinetics and fits the description given by Aziz, Aziz and Kaplan, and Aziz and Boettinger through the continuous growth model.

In spite of the strong deviation from the interfacial equilibrium, for low values of the anisotropy strength γ, the product $\rho^2 v_{\mathrm{tip}}$ scales as $\gamma^{-7/4}$, along the predictions of the free boundary model. Suppressing diffusion in the solid results in an accumulation of solute near the tip and $\rho^2 v_{\mathrm{tip}}$ decreases with increasing D_s/D_l; the opposite behavior was predicted within the free boundary model, neglecting nonequilibrium effects.

[1] D. A. Kessler, J. Koplik, and H. Levine, Adv. Phys. **37**, 255 (1988).
[2] Y. Pomeau and M. Ben Amar, in *Solids far from Equilibrium*, edited by Godreche (Cambridge University Press, Cambridge, 1992).
[3] E. A. Brener and V. I. Mel'nikov, Adv. Phys. **40**, 53 (1991).
[4] J. S. Langer, Rev. Mod. Phys. **52**, 1 (1980).
[5] P. Ivantsov, Dokl. Akad. Nauk. SSSR **58**, 567 (1947).
[6] J. S. Langer and D. C. Hong, Phys. Rev. A **34**, 1462 (1986).
[7] A. Barbieri, D. C. Hong, and J. S. Langer, Phys. Rev. A **35**, 1802 (1987).
[8] A. Barbieri and J. S. Langer, Phys. Rev. A **39**, 5314 (1989).
[9] Y. Pomeau and M. Ben Amar, Europhys. Lett. **2**, 307 (1986).
[10] M. Ben Amar, Phys. Rev. A **41**, 2080 (1990).
[11] G. Caginalp, in *Applications of Field Theory to Statistical Mechanics*, edited by L. Garrido, Lecture Notes in Physics Vol. 26 (Springer, Berlin, 1984), p. 216.
[12] G. Caginalp, in *Material Instabilities in Continuum Problems and Related Mathematical Problems*, Proceedings of the Heriot-Watt Symposium (1985–1986), edited by J. Ball (Oxford University Press, Oxford, 1988), pp. 35–52.
[13] G. Caginalp, Arch. Ration. Mech. Anal. **92**, 205 (1986).
[14] G. Caginalp, Phys. Rev. A **39**, 5887 (1989).
[15] G. Caginalp and E. A. Socolovsky, J. Comput. Phys. **95**, 85 (1991).
[16] A. A. Wheeler, W. J. Boettinger, and G. B. McFadden, Phys. Rev. A **45**, 7424 (1992).
[17] A. A. Wheeler, W. J. Boettinger, and G. B. McFadden, Phys. Rev. E **47**, 1893 (1993).
[18] G. Caginalp and W. Xie, Phys. Rev. E **48**, 1897 (1993).
[19] G. Caginalp and J. Jones, Ann. Phys. (N.Y.) **237**, 66 (1995).
[20] J. A. Warren and W. J. Boettinger, Acta Metall. Mater. **43**, 689 (1995).
[21] M. Conti (unpublished).
[22] M. Conti (unpublished).
[23] G. B. McFadden, A. A. Wheeler, R. J. Braun, and S. R. Coriell, Phys. Rev. E **48**, 2016 (1993).
[24] M. J. Aziz, J. Appl. Phys. **53**, 1158 (1982).
[25] M. J. Aziz and T. Kaplan, Acta Metall. **36**, 2335 (1988).
[26] M. J. Aziz and W. J. Boettinger, Acta Metall. Mater. **42**, 527 (1994).
[27] M. C. Flemings, *Solidification Processing* (McGraw-Hill, New York, 1974).
[28] P. Pelcè and Y. Pomeau, Stud. Appl. Math. **74**, 245 (1986).
[29] A. A. Wheeler, B. T. Murray, and R. J. Schaefer, Physica D **66**, 243 (1993).
[30] F. Marinozzi, M. Conti, and U. Marini Bettolo Marconi, Phys. Rev. E **53**, 5039 (1996).
[31] R. Willnecker, D. M. Herlach, and B. Feuerbacher, Phys. Rev. Lett. **62**, 2707 (1989).